PSFC/JA-02-10

Toroidal Rotation as an Explanation for Plasma Flow Observations in the Alcator C-Mod Scrape-Off Layer

B. LaBombard, S. Gangadhara, B. Lipschultz, C.S. Pitcher[1]

August 2002

Plasma Science and Fusion Center
Massachusetts Institute of Technology
Cambridge, MA 02139 USA

[1]Institute for Aerospace Studies, University of Toronto, Toronto, Canada

This work was supported by the U.S. Department of Energy, Cooperative Grant No. DE-FC02-99ER54512. Reproduction, translation, publication, use and disposal, in whole or in part, by or for the United States government is permitted.

Submitted for publication to *Journal of Nuclear Materials.*

Toroidal rotation as an explanation for plasma flow observations in the Alcator C-Mod scrape-off layer

B. LaBombard, S. Gangadhara, B. Lipschultz, C.S. Pitcher[a]

Plasma Science and Fusion Center
Massachusetts Institute of Technology
Cambridge, MA 02139, USA

[a]*Institute for Aerospace Studies*
University of Toronto, Toronto, Canada.

Parallel and $\underline{E} \times \underline{B}$ plasma flows near the separatrix on the outside midplane of Alcator C-Mod are investigated with a scanning probe for a range plasma densities, currents, and magnetic fields. Strong parallel flows (up to Mach 0.6) are found to peak ~2 mm into the scrape-off layer (SOL), reverse nearly symmetrically with magnetic field reversal, and decrease in magnitude with increasing line-averaged density normalized to the Greenwald density. $\underline{E} \times \underline{B}$ flows in the SOL inferred from the poloidal propagation velocity of plasma fluctuations appear to compensate these parallel flows and scale similarly, i.e., the dominant flow pattern is a pure toroidal rotation. $\underline{E} \times \underline{B}$ flows inferred by probe-sheath potentials are generally smaller, exhibit more scatter, and do not scale the same, perhaps indicating a less reliable measurement. These measurements suggest a residual poloidal flow (along field lines) of ~0.2 to ~1 times the electron diamagnetic velocity, depending on plasma conditions.

Paper presented at the 15th PSI conference, Gifu, Japan, May 27-31, 2002

1. Introduction

Plasma flow along magnetic field lines approaching a significant fraction of the plasma sound speed has been seen in scrape-off layer (SOL) regions far from material surfaces in many tokamaks [1-6]. There is renewed interest in identifying the drive mechanisms since the flows may affect the impurity compression of the divertor, the transport of impurities in the SOL plasma, and perhaps the balance of impurity erosion and redeposition between the inner and outer divertor legs.

Strong parallel flows above the outer divertor in Alcator C-Mod were reported previously [4]. Near the separatrix, the flow was found to be directed towards or away from the divertor entrance, depending on the direction of the plasma current and toroidal magnetic field. These sometimes 'reversed flows' had the appearance of poloidally circulating the plasma, suggesting that an asymmetry in divertor ionization may be partly responsible. The possible roles of divertor ionization imbalance and/or poloidal variations in cross-field transport in driving parallel flows in C-Mod is presently being considered in more detail [7]. Measurements and modeling in DITE [8], JT-60U [5], and JET [9] indicate that parallel flows in the SOL can arise from toroidal effects such as Pfirsch-Schulter ion flows, ballooning transport, and co-current toroidal momentum generation. Biasing experiments in TdeV [3] showed that the plasma tends to rotate toroidally in response to an imposed radial electric field. This response is intuitive: it is a divergence-free motion incurring minimal resistance in the axisymmetric geometry. It also does not result in net poloidal plasma or impurity flows.

In this paper, probe measurements of flow in the parallel and cross-field directions near the outside midplane on Alcator C-Mod are assembled to address the question: Does toroidal rotation simply explain the observed plasma flow pattern or are other mechanisms playing a role? Recent modeling of flows in C-Mod suggest that the outside midplane may be an ideal location for addressing this question experimentally; the flow pattern that results from the simple consideration of ionization and cross-field transport tends to exhibit a stagnation point at this location (see Ref. [7]). Parallel flow is inferred by a Mach probe while $\underline{E} \times \underline{B}$ flows are obtained from two methods: the propagation velocity of plasma fluctuations and radial electric field from

sheath potentials. Unfortunately, the latter two estimates of $\underline{E} \times \underline{B}$ flow are found to differ substantially. $\underline{E} \times \underline{B}$ flows inferred by plasma fluctuations scale similarly as and mostly cancel the poloidal projection of the parallel flows. When an allowance for finite electron temperature fluctuations is included in the estimate, the cancellation becomes nearly exact. $\underline{E} \times \underline{B}$ flows from sheath potentials also tend to cancel the poloidal projection of parallel flows but the velocities are generally smaller and do not track changes in parallel flow magnitude.

2. Experiment

A cross-section of a typical Alcator C-Mod equilibrium and the location of a horizontally scanning probe is shown in Fig. 1. Results are reported from ohmic heated deuterium discharges with plasma currents (I_p) between 0.5 and 1.0 MA, toroidal magnetic field strength (B_T) between 4 and 6 tesla, and line-averaged plasma densities, $0.8 < \bar{n}_e < 2.4$ x10^{20} m^{-3} . Data is reported from discharges with 'normal' B_T and I_p direction ($B \times \nabla B$ towards lower x-pt) and reversed B_T and I_p direction. In all cases, the plasma had a lower single-null magnetic equilibrium, similar to that shown in Fig. 1, with I_p in the direction of B_T.

A close-up view of the horizontal-scanning probe head, located 10 cm above the outer midplane, is shown in Fig. 1. Four 1.5 mm diameter tungsten electrodes with ends flush to a pyramidal surface are arranged equidistant from the peak of the pyramid and coincident with the four edges of the pyramid. The EAST and WEST electrodes sample plasma from opposite directions along the same field line, forming a 'Mach probe pair' in which the parallel Mach number can be estimated from the ratio of ion saturation currents, $M_{//} = 0.43 \ln\left(I_{east} / I_{west}\right)$ [10]. By fitting positive and negative-going *I-V* characteristics from the EAST and WEST electrodes, densities, temperatures, and parallel Mach numbers along the probe's trajectory are obtained every 0.25 ms (corresponding to ~0.25 mm of probe travel). The NORTH and SOUTH electrodes, which sample plasma from both directions on their respective magnetic field lines, were operated in a floating-voltage mode (1 MHz sample frequency). All data is mapped along flux surfaces to the distance outside the separatrix at the plasma midplane, ρ. Using SOL

power balance and electron pressure mapping constraints, the location of the separatix is determined to an accuracy of ~ 2 mm.

3. Plasma profiles and estimates of flow velocities

Density, electron temperature, floating potential, and parallel plasma flow velocity profiles are shown in Fig. 2 for a set of representative discharges. The symbol-marked curves are smooth spline fits to the many data points that are generated over the probe's trajectory. Parallel flow velocities ($V_{//}$) are computed using the Hutchinson formulation[10] and an estimate of the local plasma sound speed with $T_i \approx T_e$. Although there is experimental evidence supporting this formulation, it assumes the ratio of particle to momentum diffusivities to be unity; varying this ratio by a factor of two leads to a 20% variation in the inferred parallel flow velocities. Negative values of $V_{//}$ correspond to flow directed from outer to inner divertor surfaces.

As seen in Fig. 2, parallel flows in the SOL can be quite large; inferred values up to Mach 0.6 are routinely found at a location ~2-3 mm outside the separatrix in low density discharges. The $V_{//}$ profile peaks outside the separatrix region, implying that $V_{//}$ is generated within the SOL region itself. Figure 2 shows the evolution of the $V_{//}$ profile with plasma density. As the plasma density is raised the magnitude of the flow decreases across the entire profile.

Two different estimates are made for the cross-field plasma velocity, $v_{E\times B}$, one from the poloidal propagation of plasma fluctuations and one from the radial gradient in the inferred plasma potential profile. The poloidal phase velocity of plasma fluctuations can be computed from the NORTH and SOUTH floating potential data. A standard analysis is employed here in which the frequency and poloidal wave number-resolved fluctuation power spectrum, $S(k,\omega)$, is deduced by a two-point correlation method [11]. In general, $S(k,\omega)$ is found to exhibit a well defined elliptical shape in the (k,ω) plane, with minor axis much smaller than major axis. The slope of major axis of the ellipse is found by minimizing the $S(k,\omega)$-weighted 'moment of inertia' about that axis. This slope, which is the power-averaged poloidal phase velocity of the

plasma fluctuations, v_{ph}, is found to be reliably identified with a standard deviation of less than 20% for data taken over the SOL region $\rho \leq$ 6 mm.

It is well established that fluctuations in the edge plasma propagate with a superposition of $\underline{E} \times \underline{B}$ and drift-wave velocities,

$$v_{ph} = v_{E\times B} + v_d \quad ; \quad v_d \approx \frac{T_e}{B}\frac{\nabla_r n}{n} + \alpha \frac{\nabla_r T_e}{B} \quad . \qquad (1)$$

The parameter, α, accounts for the contribution to v_d owing to finite electron temperature fluctuations and is of order $\sim \tilde{T}_e n / \tilde{n} T_e$. Experiments [12, 13] and modeling [14, 15] indicate that this parameter is near unity in the edge plasma. In the present paper, separate $v_{E\times B}$ profiles are computed from Eq. (1) with α=0 and α=1 to explore the sensitivity to this parameter. Positive values of $v_{E\times B}$ are directed from inner to outer divertor surfaces.

From the electron temperature and floating potential profiles, V_f, the plasma potential and corresponding $v_{E\times B}$ can be estimated from a probe-sheath model,

$$\Phi = V_f + \delta T_e \quad ; \qquad v_{E\times B} = -\frac{\nabla_r \left(V_f + \delta T_e \right)}{B} \qquad . \qquad (2)$$

Parameter, δ, characterizes the sheath potential drop. For a pure deuterium plasma with Maxwellian electrons and no secondary electron emission (ion-induced, electron-induced, or thermionic), $\delta \approx$ 2.8. For the present paper, a correction to δ is included, accounting for electron-induced secondary electron emission from tungsten with a primary electron population at temperature T_e.

Figure 3 shows profiles of v_{ph}, v_d and $v_{E\times B}^{ph}$ [Eq. (1) with α=0], and $v_{E\times B}^{\Phi}$ [Eq. (2)] obtained for the discharges of Fig. 2. Although both estimates show qualitatively similar profiles, the magnitudes and trends with discharge conditions are different. Values of $v_{E\times B}^{ph}$ are generally more positive than $v_{E\times B}^{\Phi}$ and are a factor of two higher near $\rho \sim$ 2 mm, despite the fact that $v_{E\times B}^{ph}$ has been computed with α=0. Also $v_{E\times B}^{ph}$ exhibits a systematic dependence on discharge conditions, particularly near $\rho \sim$ 2 mm, while $v_{E\times B}^{\Phi}$ does not.

These differences prompt us to consider the accuracy of the inferred $v_{E\times B}$ values; both methods involve taking the difference in two quantities that have some inherent uncertainty. The probe-sheath method requires: (1) a reliable model of the sheath potential drop, δ, which must account for plasma-probe surface interaction in the presence of possible non-thermal electron effects and possible thermionic electron emission, and (2) accurate measurements of the local floating potential. A complexity arises in determining the floating potential in a flowing plasma; an 'upstream' probe will have a higher floating potential (owing to higher density, plasma potential) than a downstream probe with all other parameters being equal. (The floating potential data shown here are the average of all 4 probe elements.) In view of these difficulties, the fluctuation phase velocity method appears to have an advantage; it is insensitive to surface physics effects. Although the method does require knowledge of α, α=0 should yield a reliable lower-bound estimate of $v_{E\times B}$.

4. Comparison of parallel and poloidal flow velocities in SOL

Comparing the parallel flows in Fig.2 with the $v_{E\times B}$ flows in Fig. 3, one can see that they tend to have the opposite sign in the SOL, i.e., the poloidal components of these flows tend to cancel. In order to explore this behavior in more detail, data from a wider range of plasma conditions was assembled: 144 profiles with normal magnetic field direction and 81 profiles with reversed. For both field directions, current, field and density scans were performed: $0.5 < I_p < 1.0$ MA , $4 < B_T < 6$ tesla, $0.8 < \bar{n}_e < 2.4$ x10^{20} m^{-3}.

Figure 4 shows the full set of parallel and poloidal flow velocity profiles, colored according to discharge conditions. The parallel flow is seen to have a nearly symmetric behavior with respect to magnetic field direction: Mach number profiles peak in the range ρ ~ 2-3 mm and have largest magnitudes of around 0.6. The second panel shows the poloidal projection of the local parallel flow velocity, i.e., $B_\theta v_{//} / B$, while the remaining panels show the negative of $v_{E\times B}$ from three computations: Eq. (1) with α=0 and α=1, and Eq. (2). Curves in the last 4 panels are colored according to line-average discharge density normalized to the Greenwald

density, $\bar{n}_e / n_G$. (This parameter was chosen because edge plasma profiles and local transport conditions correlate with this quantity[16]). If $B_\theta v_{//} / B$ and $v_{E\times B}$ were to exactly cancel over all plasma conditions then those panels would look identical. Although not identical, the panels containing $B_\theta v_{//} / B$ and $-v_{E\times B}^{ph}$ (α=1) are remarkably alike, exhibiting: (1) reversal in flow direction with B_T reversal, (2) similar magnitude and profile shapes, peaking in the range ρ ~ 2-3 mm, and (3) similar dependence on $\bar{n}_e / n_G$, favoring smaller flow velocities at large $\bar{n}_e / n_G$.

Owing to the plasma current and toroidal field scans, B_θ / B at the scanning probe location was changed by a factor of 2. An important question is: as $v_{E\times B}$ varies with $\bar{n}_e / n_G$, does $B_\theta v_{//} / B$ vary proportionally for all B_θ / B values? Figure 5 shows $B_\theta v_{//} / B$ plotted versus three computations of $v_{E\times B}$ at the location ρ = 3 mm. Data points are binned into three B_θ / B groups and colored accordingly. In each panel, the horizontal and vertical axes are the same; any data falling on the dashed line would correspond to a net zero velocity in the poloidal direction. Solid black lines are drawn through the centroids of each cluster of normal or reversed B_T data points and parallel to the dashed lines. As seen in the first panel, $B_\theta v_{//} / B$ is found to track remarkably well with $v_{E\times B}^{ph}$ (α=1), independent of the value of B_θ / B. On the other hand, $B_\theta v_{//} / B$ does not track so well with $v_{E\times B}^{\Phi}$. By this measure, a residual poloidal flow of ~0.2 to 1 times the electron diamagnetic velocity (depending on plasma conditions) is suggested.

5. Conclusions

Strong parallel flows (up to Mach 0.6) are measured near the outer midplane on Alcator C-Mod that peak ~2 mm into the SOL, reverse nearly symmetrically with magnetic field, and decrease in magnitude with increasing $\bar{n}_e / n_G$. In contrast, modeling suggests that flows driven by ionization and cross-field transport mechanisms alone lead to a nearly stagnant parallel flow profile on the outer midplane [7]. Based on the poloidal propagation velocity of fluctuations, the parallel flows in the SOL appear to be compensated by $\underline{E}\times\underline{B}$ flows that scale similarly, i.e., the

overall flow pattern is nearly a pure toroidal rotation. $\underline{E} \times \underline{B}$ flows estimated from sheath potentials are found to be smaller in magnitude, scale differently with plasma conditions, and only partially compensate the parallel flows. By this measure, a residual poloidal flow (along field lines) of ~0.2 to ~1 times the electron diamagnetic velocity is indicated, depending on plasma conditions.

Acknowledgments

This work is supported by U.S. Department of Energy Contract No. DE-AC02-78-ET-51013.

References

[1] Vershkov, V.A., Grashin, S.A., and Chankin, A.V., J. Nucl. Mater. **145** (1987) 611.

[2] Pitts, R.A., Vayakis, G., Matthews, G.F., and Vershkov, V.A., J. Nucl. Mater. **176** (1990) 893.

[3] MacLatchy, C.S., et al., J. Nucl. Mater. **196** (1992) 248.

[4] LaBombard, B., et al., J. Nucl. Mater. **241-243** (1997) 149.

[5] Asakura, N., et al., Nucl. Fus. **39** (1999) 1983.

[6] Erents, S.K., Chankin, A.V., Matthews, G.F., and Stangeby, P.C., Plasma Phys. Controlled Fusion **42** (2000) 905.

[7] Pitcher, C.S., this conference.

[8] Hugill, J., J. Nucl. Mater. **196** (1992) 918.

[9] Chankin, A.V., et al., J. Nucl. Mater. **290** (2001) 518.

[10] Hutchinson, I.H., Phys. Rev. A **37** (1988) 4358.

[11] Beall, J.M., Kim, Y.C., and Powers, E.J., Journal of Applied Physics **53** (1982) 3933.

[12] Meier, M.A., Bengtson, R.D., Hallock, G.A., and Wootton, A.J., Phys. Rev. Lett. **87** (2001) 085003.

[13] Boedo, J.A., et al., Phys. Plasmas **8** (2001) 4826.

[14] Zweben, S.J., et al., Phys. Plasmas **9** (2002) 1981.

[15] Hallatschek, K., private communication.

[16] LaBombard, B., et al., Phys. Plasmas **8** (2001) 2107.

Figure Captions

Fig. 1. Parallel and cross-field flow data is recorded by a horizontal scanning probe located 10 cm above the outer midplane. The probe head employs four tungsten electrodes (1.5 mm dia.), equally spaced around the apex of a molybdenum pyramid and machined to match its surfaces. The NORTH and SOUTH probes record the poloidal dispersion of floating potential fluctuations while the EAST and WEST probes are operated in a swept-voltage mode, yielding density, electron temperature and parallel flow velocity information.

Fig. 2. Representative profiles of density, electron temperature, floating potential, and parallel flow velocity are shown. Discharge conditions are: ohmic L-mode with I_p=0.8 MA and B_T=5.3 tesla (normal directions). Line-averaged density in units of 10^{20} m^{-3} is indicated by the different symbols. All data are plotted versus distance into the scrape-off layer, mapped to the outer midplane.

Fig. 3. Profiles of plasma fluctuation phase velocity (v_{ph}), drift-wave propagation velocity (v_d) and inferred $\underline{E}\times\underline{B}$ velocity ($v_{E\times B}^{ph}$) [from Eq. (1) with α=0], and $\underline{E}\times\underline{B}$ velocity inferred from probe-sheath model ($v_{E\times B}^{\Phi}$) [Eq. (2)]. The discharges correspond to those shown in Fig. 2. $v_{E\times B}^{ph}$ and $v_{E\times B}^{\Phi}$ exhibit quantitative differences; $v_{E\times B}^{ph}$ varies strongly with discharge density while $v_{E\times B}^{\Phi}$ does not.

Fig. 4. Plasma velocity profiles inferred from 144 probe scans are overlaid: parallel Mach number, poloidal projection of parallel flow velocity, and three computations of $-v_{E\times B}$ from Eqs. (1) and (2). Profiles in the first panel are color-coded according to *B*-field direction. Profiles in the remaining panels are colored according to $\bar{n}_e / n_G$. The second and third panels are remarkably similar. By this measure, the poloidal projection of parallel flow velocity approximately cancels the $\underline{E}\times\underline{B}$ flow over a wide range of plasma conditions, i.e., the principle plasma motion near the separatrix in the SOL is a toroidal rotation.

Fig. 5. The poloidal projection of parallel plasma flow velocity is plotted versus three computations of $\underline{E}\times\underline{B}$ velocity at a location 3 mm into the SOL: $\underline{E}\times\underline{B}$ velocity from fluctuation phase velocity [Eq. (1) with α=0 and α=1], and probe-sheath potential [Eq. (2)]. Data are grouped by symbol color according to ratio of poloidal to total magnetic field at the probe location. Solid black lines are drawn through the centroids of normal and reversed magnetic field data points and parallel to dashed lines with slope of -1. The poloidal projection of parallel plasma flow velocity (top panel) is found to track remarkably well the $\underline{E}\times\underline{B}$ velocity inferred from plasma fluctuations (α=1).

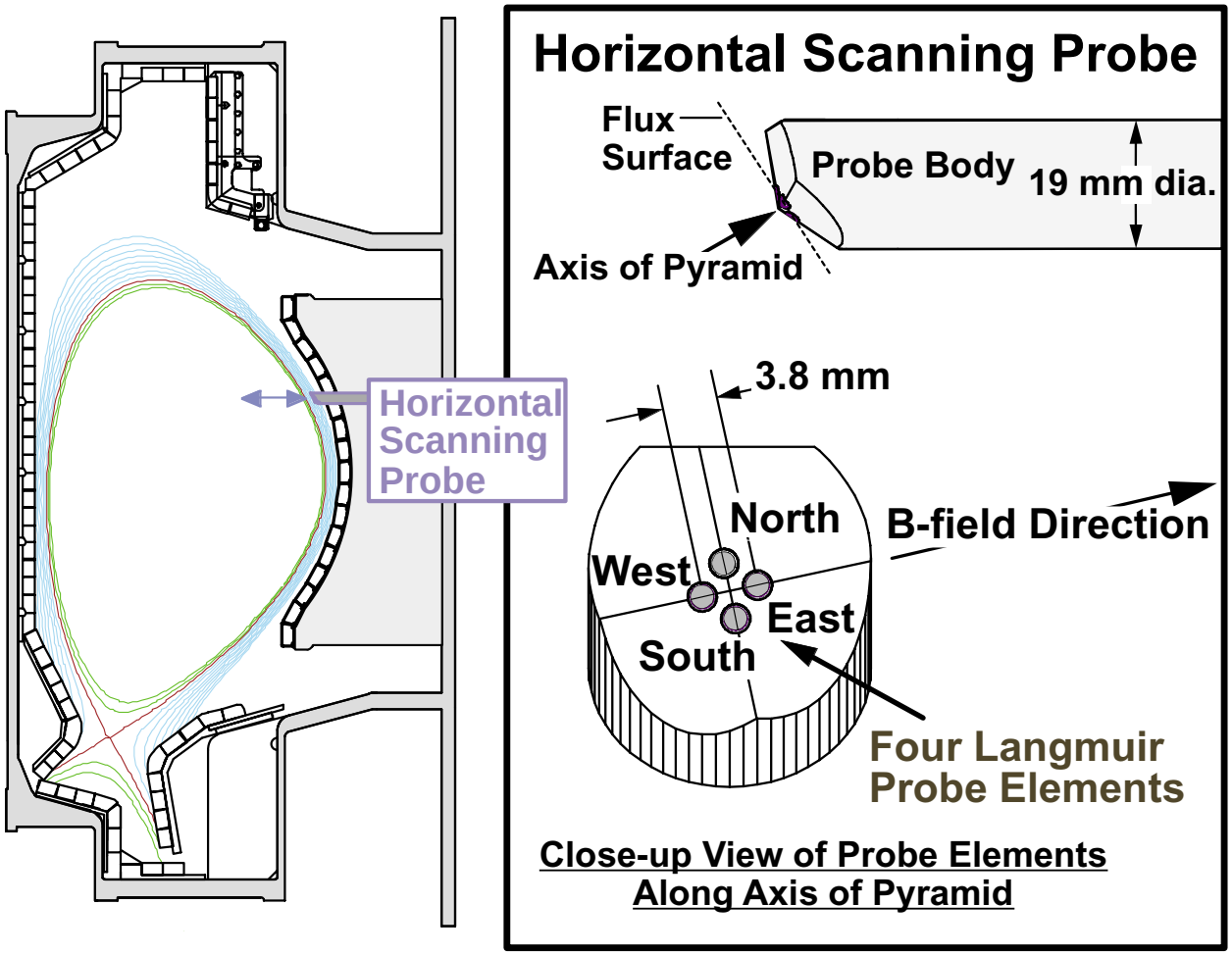

Fig. 1. Parallel and cross-field flow data is recorded by a horizontal scanning probe located 10 cm above the outer midplane. The probe head employs four tungsten electrodes (1.5 mm dia.), equally spaced around the apex of a molybdenum pyramid and machined to match its surfaces. The NORTH and SOUTH probes record the poloidal dispersion of floating potential fluctuations while the EAST and WEST probes are operated in a swept-voltage mode, yielding density, electron temperature and parallel flow velocity information.

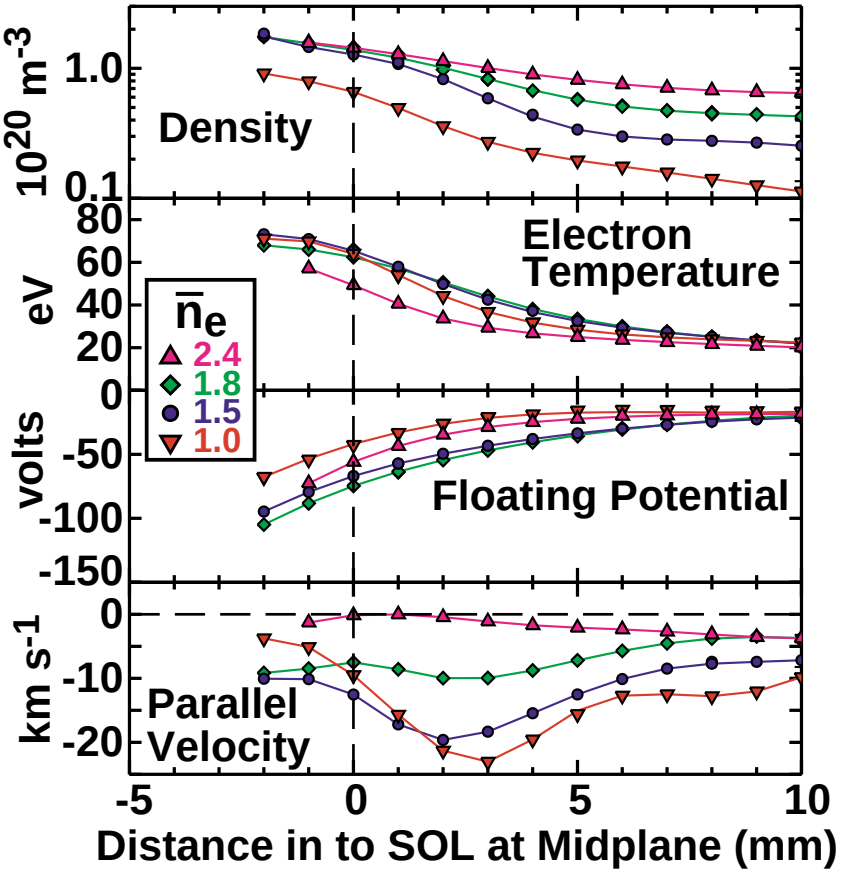

Fig. 2. Representative profiles of density, electron temperature, floating potential, and parallel flow velocity are shown. Discharge conditions are: ohmic L-mode with I_p=0.8 MA and B_T=5.3 tesla (normal directions). Line-averaged density in units of 10^{20} m^{-3} is indicated by the different symbols. All data are plotted versus distance into the scrape-off layer, mapped to the outer midplane.

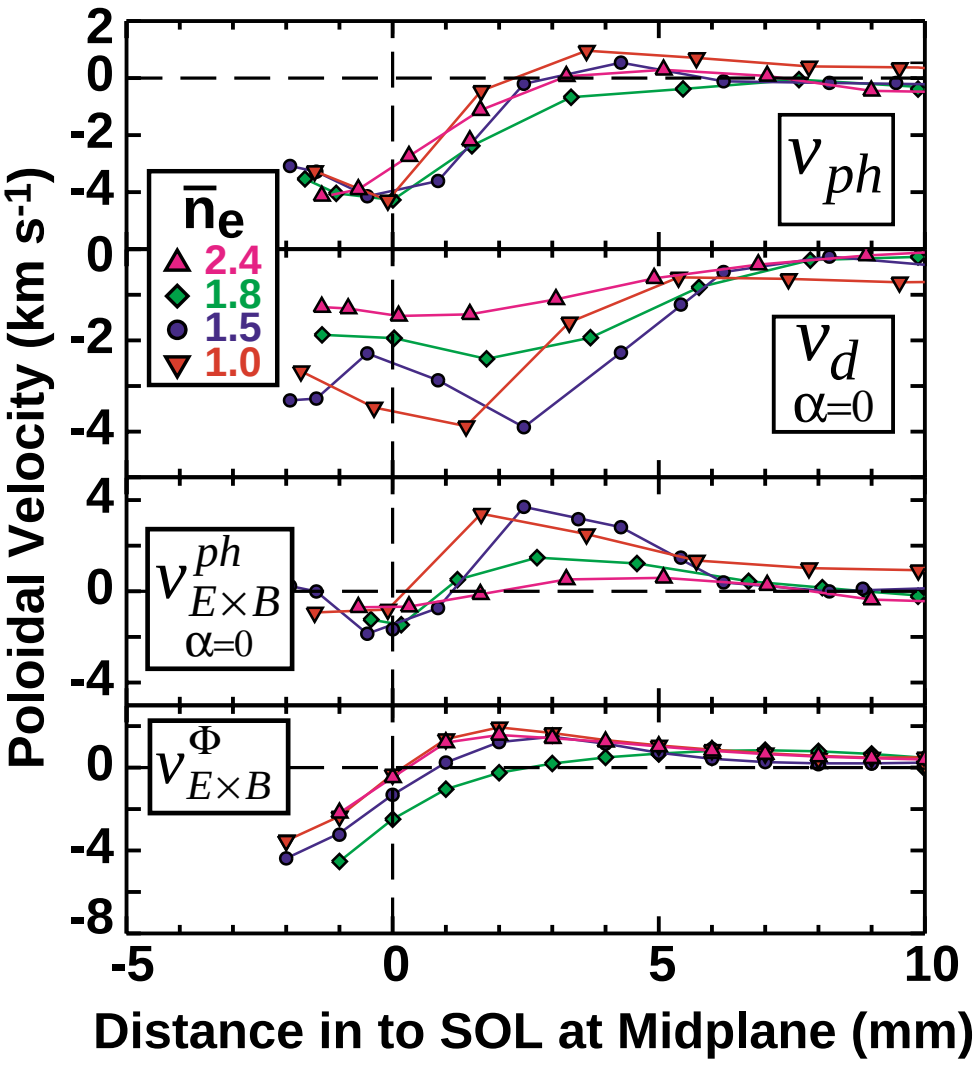

Fig. 3. Profiles of plasma fluctuation phase velocity (v_{ph}), drift-wave propagation velocity (v_d) and inferred $\underline{E}\times\underline{B}$ velocity ($v^{ph}_{E\times B}$) [from Eq. (1) with α=0], and $\underline{E}\times\underline{B}$ velocity inferred from probe-sheath model ($v^{\Phi}_{E\times B}$) [Eq. (2)]. The discharges correspond to those shown in Fig. 2. $v^{ph}_{E\times B}$ and $v^{\Phi}_{E\times B}$ exhibit quantitative differences; $v^{ph}_{E\times B}$ varies strongly with discharge density while $v^{\Phi}_{E\times B}$ does not.

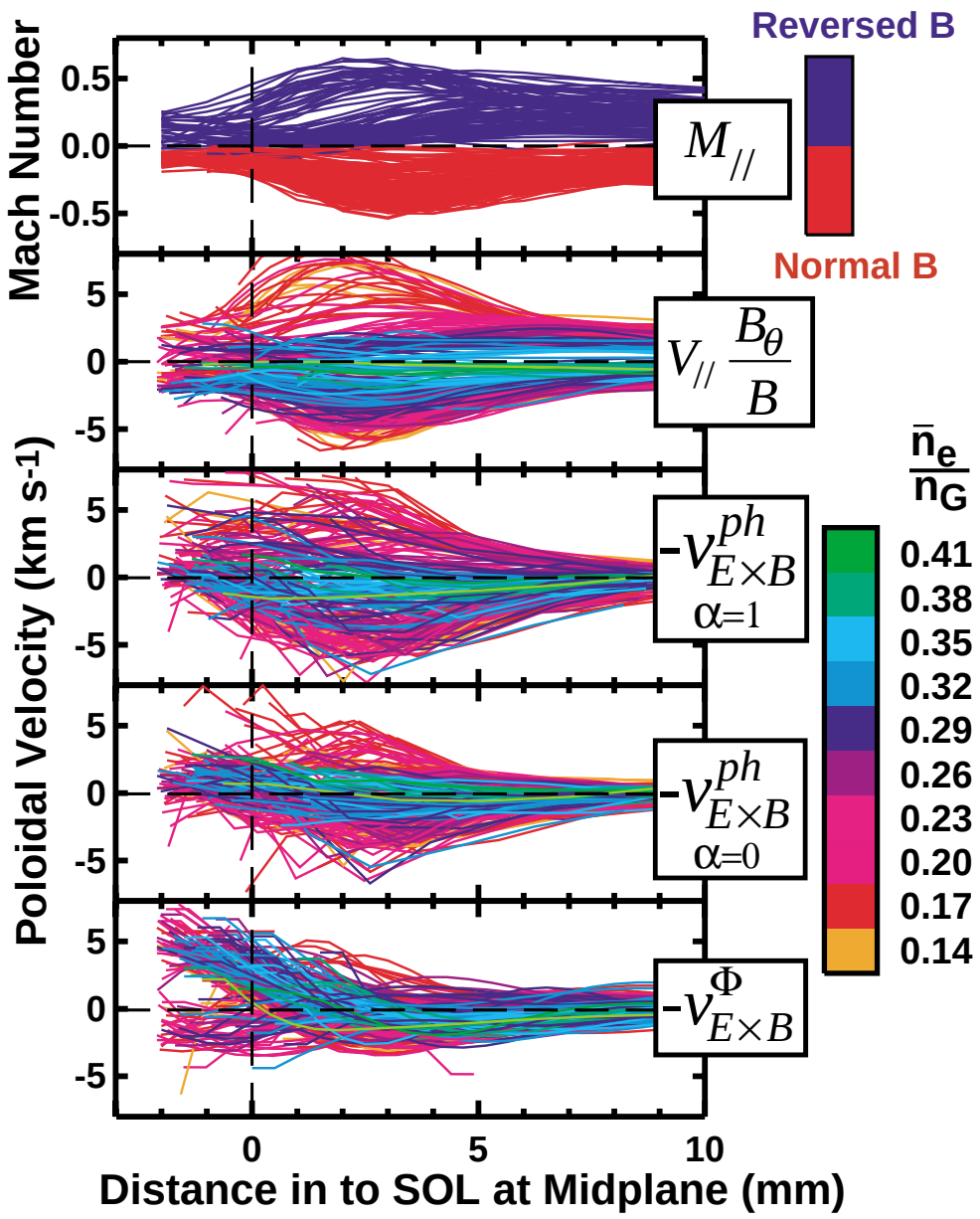

Fig. 4. Plasma velocity profiles inferred from 144 probe scans are overlaid: parallel Mach number, poloidal projection of parallel flow velocity, and three computations of $-v_{E\times B}$ from Eqs. (1) and (2). Profiles in the first panel are color-coded according to B-field direction. Profiles in the remaining panels are colored according to $\bar{n}_e / n_G$. The second and third panels are remarkably similar. By this measure, the poloidal projection of parallel flow velocity approximately cancels the $\underline{E}\times\underline{B}$ flow over a wide range of plasma conditions, i.e., the principle plasma motion near the separatrix in the SOL is a toroidal rotation.

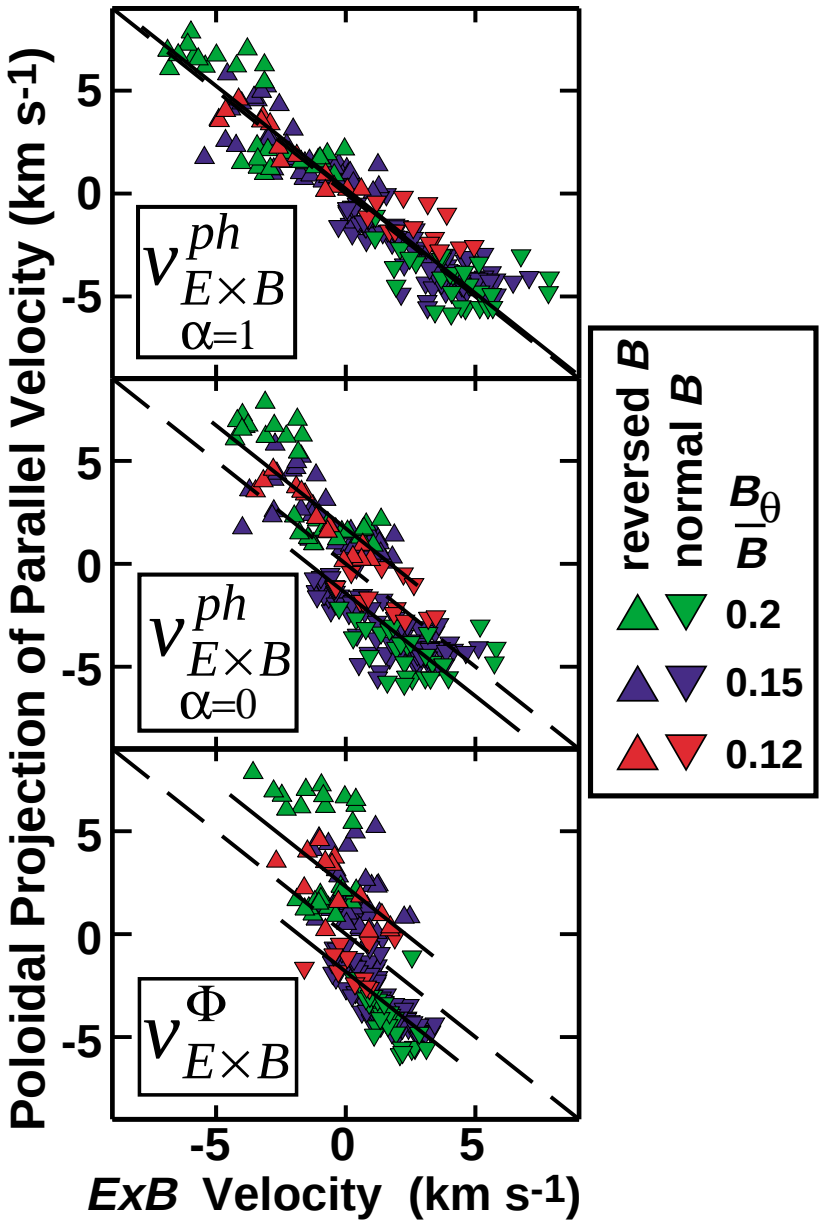

Fig. 5. The poloidal projection of parallel plasma flow velocity is plotted versus three computations of $\underline{E}\times\underline{B}$ velocity at a location 3 mm into the SOL: $\underline{E}\times\underline{B}$ velocity from fluctuation phase velocity [Eq. (1) with α=0 and α=1], and probe-sheath potential [Eq. (2)]. Data are grouped by symbol color according to ratio of poloidal to total magnetic field at the probe location. Solid black lines are drawn through the centroids of normal and reversed magnetic field data points and parallel to dashed lines with slope of -1. The poloidal projection of parallel plasma flow velocity (top panel) is found to track remarkably well the $\underline{E}\times\underline{B}$ velocity inferred from plasma fluctuations (α=1).